View Article Online / Journal Homepage / Table of Contents for this issue
Dynamic Article Links

Dalton Transactions

Cite this: *Dalton Trans.*, 2012, **41**, 13413

www.rsc.org/dalton

**PAPER**

# *In situ* EDXRD study of the chemistry of aging of co-precipitated mixed Cu,Zn hydroxycarbonates – consequences for the preparation of Cu/ZnO catalysts†

**Stefan Zander,[a] Beatrix Seidlhofer[b] and Malte Behrens*[a]**

***Received 8th June 2012, Accepted 28th August 2012***
**DOI: 10.1039/c2dt31236k**

Published on 31 August 2012 on http://pubs.rsc.org | doi:10.1039/C2DT31236K
Downloaded by Fritz Haber Institut der Max Planck Gesellschaft on 19 February 2013

In order to better understand the critical influence of the synthesis parameters during preparation of Cu/ZnO catalysts at the early stages of preparation, the aging process of mixed Cu,Zn hydroxide carbonate precursors was decoupled from the precipitation and studied independently under different conditions, *i.e.* variations in pH, temperature and additives, using *in situ* energy-dispersive XRD and *in situ* UV-Vis spectroscopy. Crystalline zincian malachite, the relevant precursor phase for industrial catalysts, was formed from the amorphous starting material in all experiments under controlled conditions by aging in solutions of similar composition to the mother liquor. The efficient incorporation of Zn into zincian malachite can be seen as the key to Cu/ZnO catalyst synthesis. Two pathways were observed: direct co-condensation of $Cu^{2+}$ and $Zn^{2+}$ into Zn-rich malachite at $5 \geq pH \geq 6.5$, or simultaneous initial crystallization of Cu-rich malachite and a transient Zn-storage phase. This intermediate re-dissolved and allowed for enrichment of Zn into malachite at $pH \geq 7$ at later stages of solid formation. The former mechanism generally yielded a higher Zn-incorporation. On the basis of these results, the effects of synthesis parameters like temperature and acidity are discussed and their effects on the final Cu/ZnO catalyst can be rationalized.

## 1. Introduction

Due to the enormous economical relevance of solid catalysts in the chemical industry,[1] their skillful synthesis and phenomenological optimization often is far more advanced than the understanding of the rationale behind the resulting individual values of synthesis parameters. Modern analytical methods can help to develop phenomenological catalyst synthesis towards knowledge-based design. The Cu-based methanol synthesis catalyst is a prominent example for this evolution.

Binary Cu/ZnO samples (Cu : Zn *ca.* 70 : 30) serve as a model system for the industrially applied $Cu/ZnO/Al_2O_3$ catalyst, which contains *ca.* 5–10 mol% $Al_2O_3$ as a structural promoter. Performance of the catalysts scales linearly with the accessible Cu surface area, but only within certain families of the Cu/ZnO catalyst, which were prepared by a similar method, *e.g.* by co-precipitation or from citric acid melts.[2] This observation highlights the crucial influence of the synthesis route on the catalytic properties of Cu/ZnO,[3] which is also termed the "chemical memory" of the system.[4] The differences among the material families are attributed to intrinsic promoting effects. Cu dispersion and intrinsic activity are beneficially influenced by the presence and homogeneous distribution of ZnO in the catalyst. Firstly, it stabilizes small Cu nanoparticles acting as a geometrical spacer between them.[5] Secondly, strong metal–oxide interactions between ZnO and Cu are assumed to contribute to the *in situ* formation of catalytically active sites. Different models for this latter synergetic effect are discussed in the literature.[6–13]

The most successful and industrially applied synthesis route of Cu/ZnO catalysts follows a multi-step procedure in which mixed metal hydroxide carbonate precursors are formed by pH- and *T*-controlled co-precipitation from aqueous Cu/Zn/(Al) nitrate solutions using soda solution as a precipitating agent.[14] Subsequently, the precipitate is aged in the mother liquor without further pH-control, filtrated, washed, dried, calcined and finally reduced to yield the active catalyst. It is described in the literature that aging is a crucial step during synthesis of the precursor and that it is essential for preparation of a successful catalyst.[4,14–17] Best catalysts have been found for co-precipitation and aging at pH 6.5 and 65 °C.[3]

In the following, we will discuss the influence of aging conditions on the properties of the catalyst prepared by this method on the basis of the recently published model of hierarchical meso- and nano-structuring of industrial methanol synthesis

[a]*Fritz-Haber-Institute of the Max-Planck-Society, Department of Inorganic Chemistry, Faradayweg 4-6, 14195 Berlin, Germany. E-mail: behrens@fhi-berlin.mpg.de; Fax: (+49)-(0)30-8413-4405; Tel: (+49)-(0)30-8413-4408*
[b]*Christian-Albrechts-University Kiel, Institute of Inorganic Chemistry, Max-Eyth-Straße 2, 24118 Kiel, Germany. E-mail: seidlhofer@ac.uni-kiel.de; Fax: (+49)-(0)431-880-1520; Tel: (+49)-(0)431-880-2094*

†Electronic supplementary information (ESI) available: *Ex situ* XRD, EDXRD, UV-Vis. See DOI: 10.1039/c2dt31236k

Downloaded by Fritz Haber Institut der Max Planck Gesellschaft on 19 February 2013
Published on 31 August 2012 on http://pubs.rsc.org | doi:10.1039/C2DT31236K

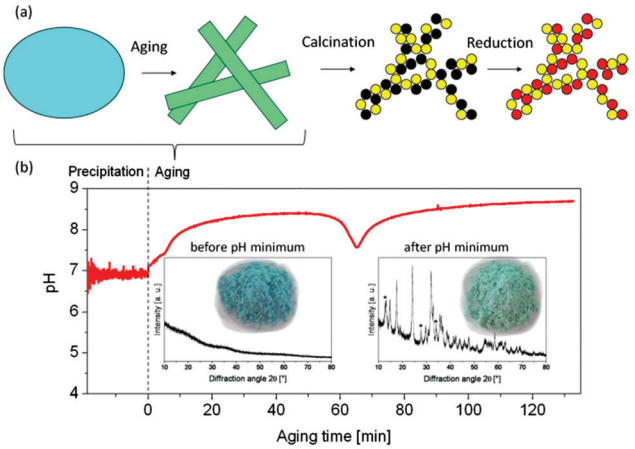


**Fig. 1** (a) Cartoon of the preparation of Cu/ZnO catalysts comprising precipitation of zincian georgeite, aging to form zincian malachite (meso-structuring), decomposition in CuO/ZnO aggregates (nano-structuring) and activation by reduction to Cu/ZnO. (b) pH evolution during precipitation and aging of a typical binary sample with change in sample color and crystallinity during aging (insets). The marked reflections in the XRD pattern refer to the aurichalcite by-phase, $(Cu,Zn)_5(OH)_6(CO_3)_2$. All other reflections are due to zincian malachite $(Cu,Zn)_2(OH)_2(CO_3)$.

catalysts, which explains the benefit of the hydroxide carbonate precursor method for preparation of Cu/ZnO catalysts (Fig. 1a).[18] In brief, the co-precipitate undergoes two micro-structure directing steps during preparation. Firstly, a mixture of zincian malachite crystallizes from the initially amorphous co-precipitate zincian georgeite[19] during aging, both with the elemental formula $(Cu,Zn)_2(OH)_2(CO_3)$.[18] This step is associated with a minimum in pH and a color change from blue to bluish green (Fig. 1b). Small amounts of aurichalcite, $(Cu,Zn)_5(OH)_6(CO_3)_2$ are often observed as a side-phase. Further aging was reported to lower the fraction of the aurichalcite phase in favor of zinc enriched malachite.[14,16] Crystallization of zincian malachite occurs preferably in the form of very thin and interwoven needles, which leads to the proper porous meso-structure. Secondly, the nano-structuring of the individual precursor needles upon thermal decomposition yields aggregates of CuO and ZnO nanoparticles. Thus, the hierarchical pore structure of the final catalyst is already predetermined at the stage of the precursor. Here, the Zn concentration in zincian malachite needles is the crucial parameter, since significant amounts of atomically distributed Zn in the joint cationic lattice of zincian malachite lead to an effective stabilization of the Cu phase in high dispersion in the decomposition product (Fig. 1a).[18] Due to solid state chemical constraints, the minimal Cu : Zn ratio in the zincian malachite phase is near 70 : 30.[20] For an efficient nano-structuring, the highest possible fraction of the available Zn amount should be incorporated into the zincian malachite precursor during aging.

The Zn fraction in this phase can be determined from the peak position of the $20\bar{1}$ reflection in the XRD pattern of zincian malachite. A low corresponding *d*-spacing is indicative of a high Zn content, which can be explained by a gradual contraction of this net plane distance caused by the average lowering of Jahn–Teller distortions of the octahedral $MO_6$ building blocks in malachite as $Cu^{2+}$ is gradually replaced by $Zn^{2+}$.[18,21] The shift of the $20\bar{1}$ reflection in the XRD pattern is, thus, a direct measure of the desired incorporation of $Zn^{2+}$ into the malachite structure and serves as an estimate of the Cu dispersion in the final catalyst.

Hence, aging, *i.e.* the period of crystalline phase formation of the precursor, plays a key role in catalyst preparation and in the so-called chemical memory of Cu/ZnO catalysts. However, the effects of synthesis parameters like pH, temperature or mother liquor composition on the precipitate are not well understood and are so far related to the catalytic performance of the resulting Cu/ZnO catalyst in a merely phenomenological manner. This lack of understanding can be seen as a major hindrance for further rational optimization of the $Cu/ZnO/(Al_2O_3)$ system and requires a systematic and fundamental study of the chemistry of precipitate aging. Such a study is complicated by the fact that variation of a given parameter affects upstream precipitation as well as aging. The ambiguity if an observed change in the properties of the precipitate is a result of modified chemistry of aging or of changes in the precipitation process (resulting in a different starting material for downstream aging) requires experimental decoupling of both events to produce a master batch of the unaged co-precipitate that can be studied during aging. In this study, we have used this approach and simulated the conditions of the aging process in the conventional catalyst synthesis with systematic variation of selected aging parameters for aliquots of the same starting material. The transformations happening during aging of the co-precipitate have been monitored by application of *in situ* methods. *In situ* energy-dispersive X-ray diffraction (EDXRD) has been shown to be a powerful method to study the mechanism[22] and kinetics[23] of solid state reactions,[24,25] *e.g.* under hydrothermal conditions[26] or in intercalation/de-intercalation reactions.[27] In this work, we have combined *in situ* EDXRD with *in situ* UV-vis spectroscopy to study the mechanism of Cu/ZnO catalyst precursor aging.

## 2. Experimental

### 2.1 Precursor preparation

Decoupling of precipitation and aging was realized by continuously feeding the initial amorphous co-precipitate slurry directly into a spray-dryer in order to suppress aging by fast drying. This "quenching technique" was necessary due to the fact that zincian georgeite is quite unstable in the mother liquor against crystallization. In the course of the preparation, constant pH co-precipitation was performed in an automated laboratory reactor (Mettler–Toledo LabMax, 2 L, prefilled with 400 mL water) at $T = 338$ K and pH 7 from a 1.6 M aqueous $Na_2CO_3$ solution and a 1 M aqueous metal nitrate solution (Cu : Zn = 70 : 30). It is noted that the conditions of co-precipitation correspond to the conventional preparation process described in the literature and were similar to the conditions of industrial catalyst preparation. A graphical representation of the precipitation log file can be found as ESI (Fig. S1†). The resulting slurry was continuously removed from the co-precipitation reactor at the rate of addition of solutions (23 mL $min^{-1}$) and directly spray-dried (Niro Minor Mobile, $T_{inlet}$ = 473 K, $T_{outlet}$ = 373 K) after an estimated residence time of less than 20 min in the reactor and the connecting

 This journal is © The Royal Society of Chemistry 2012

Downloaded by Fritz Haber Institut der Max Planck Gesellschaft on 19 February 2013
Published on 31 August 2012 on http://pubs.rsc.org | doi:10.1039/C2DT31236K

tubes. This is well below the aging period necessary for crystallization of the precursor material considering that pH minimum and color change are not expected before *ca.* 30 min of stirring in the mother liquor under these conditions.[18] Thus, the dried, solid product was X-ray amorphous except for some $NaNO_3$ resulting from crystallization of the counter ions during spray-drying (not shown). To remove $NaNO_3$ the precursor was thoroughly washed with cold water and spray-dried again leading to completely X-ray amorphous zincian georgeite. The Cu : Zn ratio of the solid was confirmed to be 73 : 27 (±2%) by XRF. The resulting precursor is referred to as "unaged" despite its residence time of 20 min in the mother liquor because of the fact that it still was amorphous. Using this procedure, which is schematically summarized in Fig. S2,† we were able to employ a batch of unaged zincian georgeite as identical starting material for aging experiments under different conditions (*T*, pH, additives) in mother liquor-analogous media without affecting the co-precipitation process.

### 2.2 *In situ* EDXRD and UV-Vis spectroscopy during simulated aging

In order to simulate the aging process, 200 mg of the precursor were suspended in 2 mL of aging solution in a glass tube (internal diameter: 10 mm; volume: 7 mL). To keep the concentrations of the relevant ions in the aging solution near the concentrations in the real mother liquor, it was freshly prepared by mixing appropriate amounts of the basic precipitating agent (1.6 M alkaline carbonate solution $A_2CO_3$, A = Na, K) and $HNO_3$ at a concentration corresponding to that of the mixed metal nitrate solution (1 M) until the desired pH was reached and stable. The *in situ* measurements were started directly after preparation of the suspension. The uncovered glass tube was placed in a metal block, whose temperature was controlled by an oil bath. The suspension inside the glass tube was stirred during the aging experiment using a magnetic stir bar.

All *in situ* aging investigations were carried out at the beamline F3 at HASYLAB/DESY, Hamburg, Germany. The beamline station receives white synchrotron radiation from a bending magnet with a critical energy of 16 keV and gives a positron beam energy of 4.5 GeV allowing detection of an energy range from 10 to 60 keV with a maximum in intensity at about 20 keV. An energy dispersive germanium detector was used to monitor the diffracted beam after transmission through the sample at a fixed angle, which was chosen as approximately 3.6° covering a *d*-spacing range of 2.6 to 12.2 Å. The beam was collimated to 100 × 100 μm. An acquisition time of 120 s yielded time-resolved X-ray powder patterns with sufficient counting statistics. The time span from placing the sample in the sample holder to the start of recording the first diffraction patterns was less than 60 s. The resulting spectra were evaluated using the EDXPowd[28] program package. More details on the experimental setup used can be found in the ESI (Fig. S3†) and literature.[29] Phase evolution was followed by plotting the integral intensity of selected well-resolved reflection as a function of time. Additionally, the change of the color of the samples was tracked by UV-Vis spectroscopy in order to monitor the conversion of blue amorphous zincian georgeite to green crystalline zincian malachite. Diffuse reflectance measurements were performed with an OceanOptics optical fiber probe placed in the suspension well above the synchrotron beam. The probe was connected with a TopSensorSystems halogen lamp and an OceanOptics high resolution spectrometer HR2000CG-UV-NIR. The acquisition time was set to 120 s per spectrum.

### 2.3 *Ex situ* characterization

All samples subjected to EDXRD measurements were cooled to room temperature after the *in situ* experiments within 5 min, filtrated and washed with water. Conventional X-ray diffraction (XRD) measurements were performed with a STOE STADI P transmission diffractometer equipped with a primary focusing Ge monochromator (Cu-$K_{\alpha 1}$ radiation) and a position-sensitive detector to determine the peak positions more accurately than was possible with EDXRD. All XRD patterns are presented as ESI (Fig. S4†). The samples were mounted in the form of a clamped sandwich of small amounts of powder fixed with a small amount of grease between two layers of a thin polyacetate film. Refinements were done in the $2\theta$ range 4–80° using the software package TOPAS.[30] Domain sizes were determined from the XRD peak widths and are given as volume weighted mean column heights. Surface area determination was performed in a Quantachrome Autosorb-6 machine by $N_2$-adsorption–desorption using the BET method. Cu : Zn ratios of the samples were obtained from X-ray fluorescence (XRF) measurements using a Bruker S4 Pioneer X-ray spectrometer.

## 3. Results and discussion

### 3.1 General

Using the method of sample preparation described in the Experimental section allowed simulating the aging process of an amorphous binary zincian georgeite co-precipitate under controlled conditions similar to those used in the course of preparation of industrial methanol synthesis catalysts (Fig. 1). *In situ* EDXRD and UV-Vis measurements allowed insight into the chemistry of aging, which is of crucial importance for the phase formation of the catalyst precursor and, thus, for the preparation of highly active catalysts.

The catalyst precursor was aged at different temperatures (323–343 K), starting acidities (pH 5.0–8.0) and using different counter cations ($Na^+$ and $K^+$). SEM revealed that during aging the morphology of the precipitate has changed from roundish particles of approximately 100–200 nm in diameter to smaller rod- and needle-like crystallites (ESI, Fig. S5†). Crystalline zincian malachite $(Cu,Zn)_2(OH)_2(CO_3)$ was finally detected by XRD after aging for all conditions applied (ESI, Fig. S4†). It is interesting to note that minor amounts of aurichalcite are typically observed for the Cu : Zn ratio of 70 : 30, *e.g.* after aging in a conventional 2 L batch reactor at 338 K and pH of 7.0 (see also marked reflections in Fig. 1b).[18] The presence of aurichalcite was barely detectable in the samples after simulated aging by *ex situ* XRD (ESI, Fig. S4†). Inclusion of the aurichalcite phase in the Rietveld fits led to improved *R*-values for some samples and resulted in varying amounts of aurichalcite between

Downloaded by Fritz Haber Institut der Max Planck Gesellschaft on 19 February 2013
Published on 31 August 2012 on http://pubs.rsc.org | doi:10.1039/C2DT31236K

**Table 1** Summary of aging parameters and aging results. The sample ID 0 refers to the unaged precursor

| | Aging conditions | | | *In situ* results (EDXRD data) | | | *Ex situ* results (recovered samples after EDXRD measurement) | | | | | |
|---|---|---|---|---|---|---|---|---|---|---|---|---|
| ID | pH | $T$ [K] | $A^+$ in $A_2CO_3$ | Na,Zn inter-mediate | Onset [min] | Reaction time[a] [min] | Aurichalcite [wt%] (± 5%) | $d_{20\bar{1}}$ [Å] | Zn inzM[b] [%] | BET [$m^2\ g^{-1}$] | FWHM-LVol[c] [nm] | Cu : Zn [mol%] (±2%) |
| 0 | — | — | — | — | — | — | — | — | — | 15 | — | 73.3 : 26.7 |
| 1 | 5 | 333 | $Na^+$ | — | 20 | — | 6 | 2.757 | 29.2 | 85 | 9.9 | 73.2 : 26.8 |
| 2 | 6 | 333 | $Na^+$ | — | 34 | — | 8 | 2.759 | 28.5 | 81 | 9.7 | 72.3 : 27.7 |
| 3 | 6.5 | 333 | $Na^+$ | — | 36 | — | 8 | 2.760 | 28.4 | 83 | 10.0 | 72.8 : 27.2 |
| 4 | 7 | 333 | $Na^+$ | X | 12 | 30 | 0 | 2.767 | 26.2 | 82 | 9.6 | 73.8 : 26.2 |
| 5 | 7.5 | 333 | $Na^+$ | X | 12 | 34 | 0 | 2.767 | 26.3 | 80 | 9.8 | 72.1 : 27.9 |
| 6 | 8 | 333 | $Na^+$ | X | 14 | 34 | 0 | 2.768 | 26.0 | 83 | 9.6 | 72.5 : 27.5 |
| 7 | 7 | 323 | $Na^+$ | X | 24 | 98 | 0 | 2.775 | 23.8 | 81 | 9.2 | 73.9 : 26.1 |
| 8 | 7 | 343 | $Na^+$ | X | 6 | 16 | 0 | 2.765 | 26.7 | 72 | 10.9 | 73.9 : 26.1 |
| 9 | 7 | 333 | $K^+$ | — | 56 | — | 13 | 2.767 | 26.2 | 77 | 9.8 | 72.3 : 27.7 |
| 10 | 7 | 343 | $K^+$ | — | 18 | — | 11 | 2.775 | 23.8 | 69 | 10.0 | 72.0 : 28.0 |

[a] Time interval between appearance and complete consumption of the intermediate. [b] Zn content in zincian malachite (zM) calculated from $d_{20\bar{1}}$ values; see also Fig. 7. [c] Crystallite sizes of zincian malachite determined from the half width of the XRD peaks using the TOPAS refinement software.

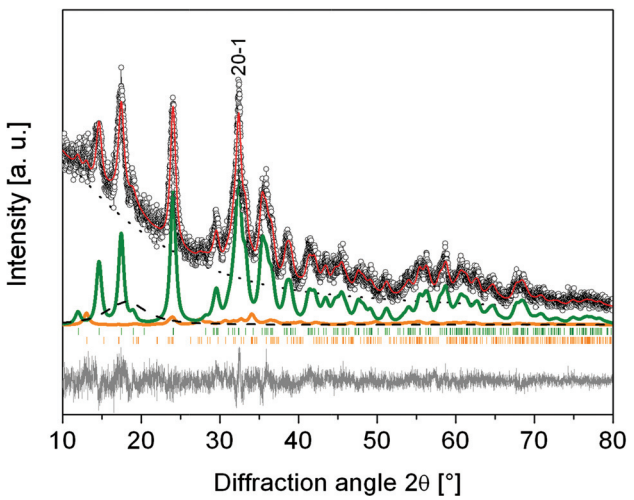


**Fig. 2** Rietveld refinement of the *ex situ* XRD pattern of the sample aged *in situ* at pH 6.5 and 333 K (ID 3) for quantitative analysis of the phase composition. Experimental data (circles), background (dotted), background peak (dashed, due to the grease used as a sticking agent to keep the sample in place on the sample holder), calculated pattern zincian malachite (green), calculated pattern aurichalcite (orange), total calculated curve (red) and difference curve (grey, offset −100). This plot is representative for the other aged samples. In this case the ratio of zincian malachite to aurichalcite was calculated to be 92% to 8%.

0 and 13 wt% (Table 1). However, due to the poor crystallinity of the sample and the low amount of this phase the error is estimated to be at least ±5 wt%. A typical graphical representation of a typical Rietveld fit is given in Fig. 2. In addition to the small differences in phase composition among the aged samples, variations in crystallinity, Zn content of the zincian malachite phase and specific surface area as a result of different aging conditions are reflected in the XRD domain sizes scattering between 9.2 and 10.9 nm, the $d_{20\bar{1}}$ value ranging between 2.757 and 2.775 Å and the BET surface areas being between 69 and 85 $m^2\ g^{-1}$ (Table 1). These observations confirm the sensitivity of relevant properties of the Cu,Zn precursor to the exact conditions of crystallization for the same starting material and a systematic discussion will be given in the following.

### 3.2 Phase evolution

The phase evolution during precursor aging will be discussed for the experiment conducted at $T$ = 323 K and pH 7.0 using a $Na^+$ containing aging solution (ID 7 in Table 1). Despite the X-ray amorphous dry starting material, some very weak XRD peaks are already observed in the first *in situ* pattern of the slurry recorded after less than 180 s after starting the experiment (Fig. 3a).

After some minutes of aging, a steep increase in Bragg peak intensity is observed and two phases can be clearly distinguished (Fig. 3b): sodium zinc carbonate, $Na_2Zn_3(CO_3)_4{\cdot}3H_2O$,[31] and the target material zincian malachite, $(Cu,Zn)_2(OH)_2(CO_3)$.[32] At the end of the experiment, only zincian malachite was observed as the final product (Fig. 3c). Sodium zinc carbonate $Na_2Zn_3(CO_3)_4{\cdot}3H_2O$ has been reported before in the literature in the context of Cu/ZnO catalyst preparation. It was identified as the initial precipitate in Zn-rich or pure Zn systems, which upon aging transformed into aurichalcite or hydrozincite.[15,33] In one study, it has probably also been detected in a Cu-rich system as a transient phase during aging,[34] but was assigned as "crystalline zincian georgeite".

One suitable, well resolved peak of both phases was chosen for further EDXRD data evaluation. The phase fraction of zincian malachite was represented by the integral intensity of the $20\bar{1}$ peak, sodium zinc carbonate by the 222 peak. The phase evolution with time is shown in Fig. 4a. The sodium zinc carbonate phase crystallizes in parallel to the zincian malachite phase and re-dissolves upon prolonged aging. The onset of crystallization occurs after 24 min and the re-dissolution of the sodium zinc carbonate occurs over 98 min without a significant increase in the zincian malachite phase.

The amorphous starting material ("zincian georgeite") is hard to comprehensively characterize. IR-spectroscopic studies of the

 This journal is © The Royal Society of Chemistry 2012

Downloaded by Fritz Haber Institut der Max Planck Gesellschaft on 19 February 2013
Published on 31 August 2012 on http://pubs.rsc.org | doi:10.1039/C2DT31236K

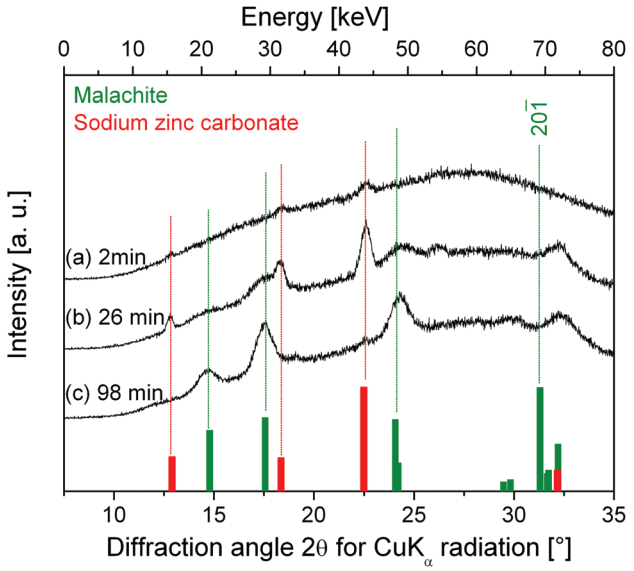


**Fig. 3** EDXRD patterns (converted to °2$\theta$ values of Cu $K_\alpha$ radiation) during aging of the amorphous precursor at pH 7 and 323 K (ID 7) after two (a), 26 (b) and 98 min (c). At the bottom PDF 72–75 (green bars) and PDF 1–457 (red bars) are shown as references for zincian malachite $(Cu,Zn)_2(OH)_2(CO_3)$ and for sodium zinc carbonate $Na_2Zn_3(CO_3)_4{\cdot}3H_2O$, respectively. The *in situ* EDXRD spectra are representative for all conducted experiments. The position of the $20\bar{1}$ peak of zincian malachite is shifted compared to the pure malachite reference because of zinc incorporation (see the text).

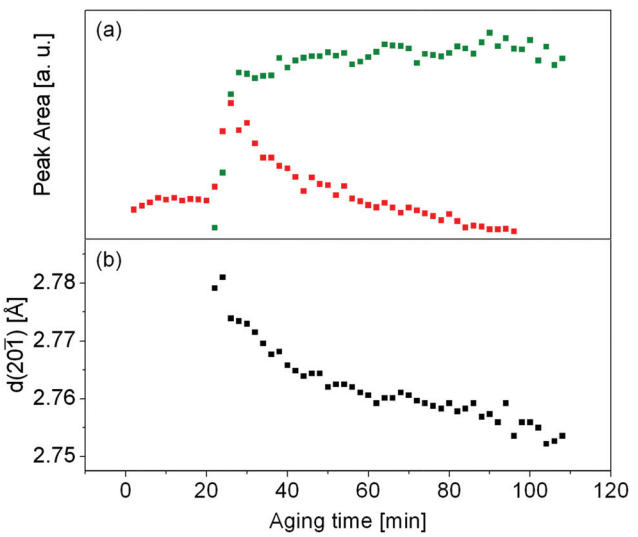


**Fig. 4** (a) Integral intensity of selected EDXRD peaks of detected phases *vs.* aging time; in $Na_2CO_3$; pH = 7; $T$ = 323 K (ID 7). Zincian malachite, $(Cu,Zn)_2(OH)_2(CO_3)$, is represented by the $20\bar{1}$ peak (green), sodium zinc carbonate $Na_2Zn_3(CO_3)_4{\cdot}3H_2O$ by the 222 peak (red). (b) Corresponding *d*-spacing of the $20\bar{1}$ peak of zincian malachite.

unaged material have shown the presence of both hydroxide as well as carbonate anions.[4,19] Here, we describe the starting precipitate as an amorphous double-salt with unknown anionic composition: $a\text{-}Cu_{0.7}(OH)_x(CO_3)_{0.7-x/2}{\cdot}Zn_{0.3}(OH)_y(CO_3)_{0.3-y/2}$. In the presence of varying amounts of $H_2O$, $OH^-{}_{aq}$ and $CO_3^{2-}{}_{aq}$ we can write for the two steps of the aging reaction:

$$\begin{aligned} &a - Cu_{0.7}(OH)_x(CO_3)_{0.7-x/2} \cdot Zn_{0.3}(OH)_y(CO_3)_{0.3-y/2} + z{Na^+}_{aq} \\ &\rightarrow (Cu_{>0.7}Zn_{<0.3})_2(OH)_2CO_3 + z/2\ Na_2Zn_3(CO_3)_4 \cdot 3H_2O \\ &\rightarrow (Cu_{0.7}Zn_{0.3})_2(OH)_2CO_3 + z{Na^+}_{aq} \end{aligned} \quad (1)$$

If we assume $Na_2Zn_3(CO_3)_4{\cdot}3H_2O$ to be a pure Zn-phase with no Cu incorporation, the initially formed zincian malachite should be poor in Zn. In the following aging step, the sodium zinc salt acts as a Zn storage phase slowly deliberating its Zn content by dissolution. This fraction of Zn can either re-precipitate in the form of a Zn-phase not detectable by XRD, or – as proposed in eqn (1) – it can be incorporated into zincian malachite by re-crystallization increasing the Zn-content of this phase. The latter possibility is supported by the evolution of the $20\bar{1}$ peak position (Fig. 4b). As the Zn storage phase re-dissolves, the peak is shifted to a lower *d*-spacing, indicating further incorporation of Zn into zincian malachite. It is noted, however, that a final proof of this mechanism is still lacking as there is a peak overlap of the $20\bar{1}$ of zincian malachite around 32.8° 2$\theta$ (for Cu $K_\alpha$ radiation) and the 422 of the sodium zinc salt located at 32.2° 2$\theta$ according to PDF 1–457. The intensity ratio of these two peaks is around 5 : 1 in this stadium. Diminishing of the latter peak due to dissolution may alone result in an artificial profile shift to higher angles in the EDXRD patterns. Unfortunately, the quality of the *in situ* EDXRD patterns is not sufficient for a whole pattern refinement. After all, the above made assumption of an intrinsic peak shift of the $20\bar{1}$ of zincian malachite seems reasonable, because no narrowing of the peak profile with time was observed, which would be associated with decrease of a shoulder (see ESI, Fig. S6†). Furthermore, the intensity of the 422 of sodium zinc carbonate is only 20% of the most intensive reflection of that phase, while the $20\bar{1}$ of zincian malachite is the strongest reflection of this phase. In Fig. 3a, where only the sodium zinc carbonate phase is present, no significant intensity due to the 422 can be seen at a position corresponding to *ca.* 32° 2$\theta$ for Cu $K_\alpha$, suggesting that the contribution of the overlapping to the peak position of the phase mixture has only a minor influence.

The UV-Vis diffuse reflectance spectra of the suspension corresponding to the starting material and the final product (aging conditions pH 7, 323 K, ID 7) are shown in Fig. 5a. The change of the position of the broad signal from 505 to 515 nm reflects a change in crystal field splitting around the $Cu^{2+}$ ions and the transition from blue to bluish green.[35] Difference plots of the normalized *in situ* recorded spectra are shown in Fig. 5b. It can be seen that several smaller bands contribute to the spectra. The presence of an isosbestic point near 510 nm was observed for all experiments and suggests that the starting material directly transforms into a single optically active product. This does not contradict the transient presence of the sodium zinc carbonate phase, but rather confirms the assumption that this phase does not contain $Cu^{2+}$ ions and does not contribute to reflectance in the Vis-range of the optical spectrum. The green part of the spectrum does hardly change and it can be seen that the change of color from blue to green is mostly due to an increase in reflectance in

Downloaded by Fritz Haber Institut der Max Planck Gesellschaft on 19 February 2013
Published on 31 August 2012 on http://pubs.rsc.org | doi:10.1039/C2DT31236K

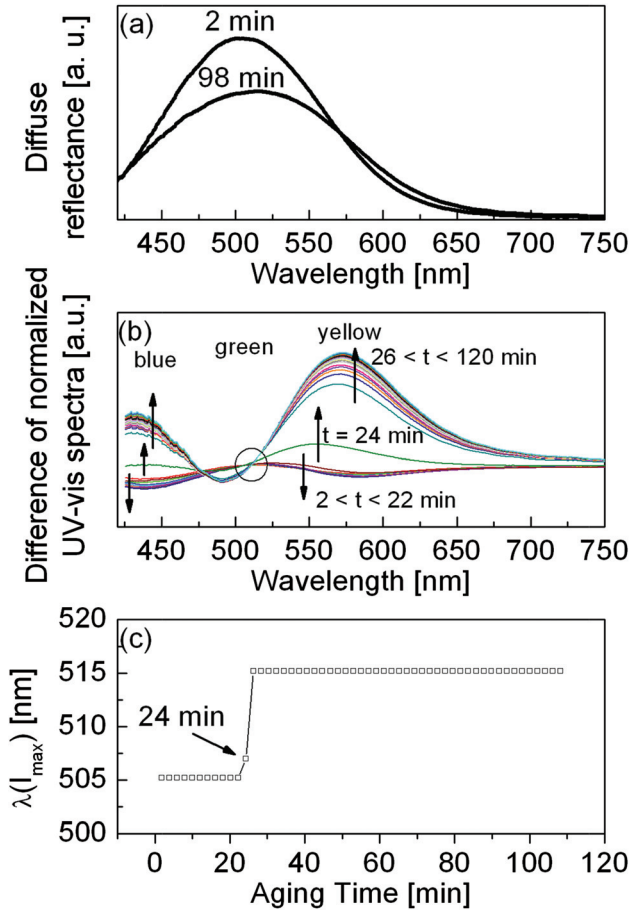


**Fig. 5** UV-vis results for simulated aging in $Na_2CO_3$ at pH 7; 323 K (ID 7). (a) Measured diffuse reflectance before and after aging. (b) Difference of normalized spectra relative to the initial spectrum at $t$ = 2 min. (c) Wavelength of the maximum intensity in the UV-vis spectra in the range of 425 to 900 nm as a function of time.

the yellow regime of the spectrum, which is much stronger compared to the increase in the blue part. The temporal evolution of the UV-vis spectrum shows only minor changes in the beginning of the reaction up to aging times of 22 min. During this period a slight decrease of reflectance in the yellow and blue part is observed, which started directly as the starting material was in contact with the aging medium. In accordance with the EDXRD results, abrupt changes occur at an aging time of 24 min and reflectance in these parts of the spectrum sharply increases. Interestingly, the color change is finished almost immediately (after less than 4 min) and again only little changes are observed at $26 < t < 120$ min, while the process of phase formation observed by EDXRD persists for 98 min. This clearly shows that the change of the color of the precursor slurry is not a suitable indicator for the end of the chemical changes happening during aging. UV-vis spectroscopy probes changes on the molecular level, which naturally precede the detection with an (ED)XRD technique as crystallization requires "oversaturation" of the newly formed complexes, which happens over a longer time scale under the conditions applied. In Fig. 5c, the maxima of the broad reflectance signal are shown as a function of aging time, showing again the step-like change at the time of crystallization of malachite.

No residual sodium zinc carbonate or other by-phases were detected after 120 min of aging. In particular, no aurichalcite was detected in the *in situ* EDXRD patterns. Aurichalcite might play a similar role as a Zn-uptake phase during aging.

Waller *et al.*[14] investigated the aging mechanism of a Cu : Zn = 67 : 33 system and observed that at first a mixture of crystalline zincian malachite (Cu : Zn ≈ 85 : 15) and aurichalcite (Cu : Zn ≈ 60 : 40) was formed and subsequently transformed into zinc richer malachite (Cu : Zn ≈ 67 : 33) at the expense of aurichalcite. We previously found that for conventional batch aging of binary precursors (Cu : Zn = 70 : 30) for 2 h at 338 K low amounts of the zinc richer phase aurichalcite co-exist with zincian malachite showing a Zn content of 27%.[18,20] As mentioned above, low amounts of aurichalcite were detected by *ex situ* XRD indicating that this phase indeed may act as a stable sink for Zn, but its amount probably is too little to be detected by *in situ* XRD or that it has crystallized only upon drying of the samples.

### 3.3 The effect of temperature

At an aging temperature of 323 K, the sodium zinc carbonate storage phase was re-dissolved within 16–98 min upon aging at pH 7.0, depending on the temperature (Fig. 4a and 6a,b, Table 1, ID 7, 4, 8). The change of the color, assigned to the beginning formation of crystalline zincian malachite, always occurred within a few minutes and was tracked by UV-Vis-spectroscopy (Fig. 5c).

Increasing the temperature from 323 K to 333 or 343 K changed the kinetics of aging and led to an earlier onset of crystallization and a shorter time period of existence of the sodium zinc phase (Fig. 6a,b and Table 1, ID 4, 7 and 8), but no changes in the mechanism of aging were observed. The monotonous shift to lower $d_{20\bar{1}}$ values (Fig. 6e and f) indicates the incorporation of Zn into zincian malachite with time after crystallization. *Ex situ* XRD was applied on the recovered samples, which allows for a more accurate determination of the absolute peak positions than *in situ* EDXRD due to higher instrumental resolution, longer acquisition time, more precise calibration and lower contribution of the background. The effect of temperature on the final degree of Zn incorporation into zincian malachite is reflected in the shift

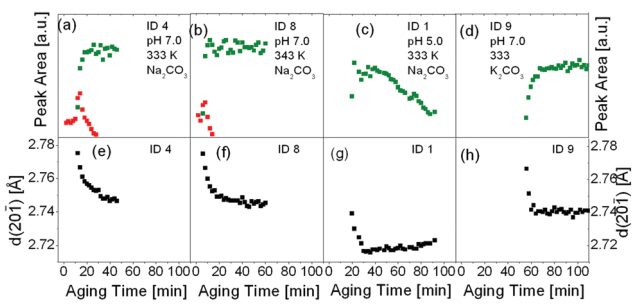


**Fig. 6** Measured features *vs.* aging time for samples noted in the plot (*cf.* Table 1). Top row a–d: Integral intensity of selected EDXRD peaks of zincian malachite (20$\bar{1}$) (green) and sodium zinc carbonate (222) (red). Bottom row e–h: Evolution of $d_{20\bar{1}}$ values of zincian malachite.


This journal is © The Royal Society of Chemistry 2012

Downloaded by Fritz Haber Institut der Max Planck Gesellschaft on 19 February 2013
Published on 31 August 2012 on http://pubs.rsc.org | doi:10.1039/C2DT31236K

of the $d_{20\bar{1}}$ spacing (Table 1, ID 4, 7 and 8). While $d_{20\bar{1}}$ was similar for the higher temperatures, it was found to be significantly larger for the zincian malachite sample prepared at 323 K indicating a lower final degree of Zn incorporation at this temperature. This observation shows that, despite stemming from the same amorphous starting material, the degree of Zn incorporation can be affected by the aging conditions. The detrimental effect of low preparation and aging temperatures has been reported in the literature.[3,36] A lack of Zn has been also observed for ternary $Cu/ZnO/Al_2O_3$ catalysts prepared at low pH or low temperature.[3] Our results suggest that this effect can be explained with a lack of Zn in the zincian malachite precursor phase. This is consistent with observations recently made during titration experiments[37] showing that the precipitation pH of $Zn^{2+}$ is shifted to higher pH values as temperature decreases. Thus, the applied aging pH may not be sufficiently basic to keep all Zn in the solid state at low temperatures and $Zn^{2+}$ may be leached out of the precipitate at low temperatures and pH values. Interestingly, XRF measurements of the sample recovered after aging at different temperatures all showed the same average Cu : Zn ratio near 70 : 30 (Table 1). This result is in agreement with local EDX measurements of the selected sample presented in the ESI (Table S2†). We thus conclude that the final pH is high enough to completely precipitate $Zn^{2+}$ also at 323 K, but suggest that during the crystallization process, which is associated with an intermediate minimum in pH peaking roughly a full pH unit below the initial aging pH under these conditions[18] (Fig. 1b), a transient leaching of $Zn^{2+}$ from the starting material may occur at low temperatures during the pH minimum. This can explain a lack of Zn in the zincian malachite phase due to (partial) Zn dissolution at the time of its crystallization. Later re-precipitation leads to formation of low amounts of undetected Zn-rich phases resulting in the same average composition, but in an inhomogeneous and thus unfavorable Zn distribution in the product.

Thus, eqn (1) has to be revised as $(Cu_{0.7}Zn_{0.3})_2(OH)_2CO_3$ is not an appropriate representation of the final product, which exhibits variations in its Cu : Zn ratio. We add an unknown Zn phase denoted Zn↓ as sink for "extra-lattice" Zn. The nature of this phase may be residual but undetected sodium zinc carbonate, amorphous or due to low abundance undetectable crystalline aurichalcite or another form of Zn-containing hydroxide or basic carbonate. Unfortunately, further structural characterization of this phase by electron microscopy or element-specific techniques is complicated due to the finely dispersed state of this phase and the large amount of Zn-containing malachite in the sample. As a function of the aging conditions this phase is present in various amounts and affects the Cu : Zn ratio in zincian malachite by limiting the available amount of Zn:

$$\begin{aligned} &\mathrm{a} - \mathrm{Cu}_{0.7}(\mathrm{OH})_x(\mathrm{CO}_3)_{0.7-x/2} \cdot \mathrm{Zn}_{0.3}(\mathrm{OH})_y(\mathrm{CO}_3)_{0.3-y/2} + z\mathrm{Na}^+_{\mathrm{aq}} \\ &\rightarrow (\mathrm{Cu}_{\gg 0.7}\mathrm{Zn}_{\ll 0.3})_2(\mathrm{OH})_2\mathrm{CO}_3 + z/2\ \mathrm{Na}_2\mathrm{Zn}_3(\mathrm{CO}_3)_4 \cdot 3\mathrm{H}_2\mathrm{O} \\ &\rightarrow (\mathrm{Cu}_{>0.7}\mathrm{Zn}_{<0.3})_2(\mathrm{OH})_2\mathrm{CO}_3 + z\mathrm{Na}^+_{\mathrm{aq}} + w\mathrm{Zn}\downarrow \end{aligned} \quad (2)$$

A quantification of the Zn-content in the final zincian malachite phase is possible by assuming a Vegard-type behavior of this lattice spacing and calibrating the obtained $d_{20\bar{1}}$ values with reference values from (zincian) malachite samples far from its limit of Zn incorporation. This is shown in Fig. 7. If the data points are arranged on the extrapolated line, they cover variations in the Zn-content of zincian malachite between 23.8 and 29.2% Zn as a function of different aging conditions (Table 1). The largest Zn-contents determined with this method are very close to the nominal Cu : Zn-ratio applied during synthesis of 70 : 30, but exceed the Zn-content of the starting material determined by XRF. This discrepancy is attributed to the difference of the two methods and their calibration errors. In the case of the sample obtained at 323 K the Zn content in zincian malachite is only 23.8%, while the rest of the Zn is trapped in a relatively large amount of the Zn-sink phase Zn↓. At 333 or 343 K, the amount of Zn↓ is lower and the Zn-content in zincian malachite is 26.2 and 26.7%, respectively.

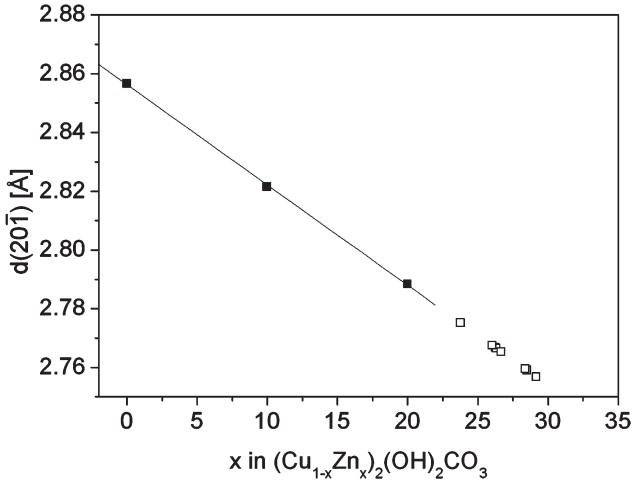


**Fig. 7** Calibration of the $d_{20\bar{1}}$ values *versus* the Zn content in zincian malachite. The three solid data points stem from reference samples described in ref. 18 and 21 and were used for linear extrapolation. The open data points positioned onto the extrapolated line refer to the values observed in this study (from *ex situ* XRD). The resulting Zn-contents are given in Table 1.

It is noted that a beneficial effect of lowering the temperature on the crystallite size is observed, which decreases with temperature from 10.9 nm at 343 K to 9.2 nm at 323 K. Accordingly, the lowest BET surface areas were found for the samples prepared at 343 K (Table 1).

In summary, the effect of increasing temperature accelerates the crystallization kinetics, leads to larger crystallites and, thus, is detrimental for the meso-structure of the catalyst precursor. Lowering the temperature to 323 K, however, leads to intermediate leaching of $Zn^{2+}$ from the co-precipitate and to an unfavorable Zn distribution resulting in a lower degree of Cu,Zn-substitution of the zincian malachite phase. This hinders an effective nano-structuring of the catalyst. Thus, the empirically optimized aging temperature around 338 K can be understood from the chemistry of aging of the precursor and envisaged as the optimum of two antagonistic trends.

### 3.4 The effect of acidity

The effect of different pH values during aging was investigated at 333 K with $Na^+$ containing aging solutions. The phase

Downloaded by Fritz Haber Institut der Max Planck Gesellschaft on 19 February 2013
Published on 31 August 2012 on http://pubs.rsc.org | doi:10.1039/C2DT31236K

evolution data for aging at pH 7.0 are shown in Fig. 6a and only minor differences were observed if the experiment was conducted at a higher pH of 7.5 or 8.0 (Table 1, ID 4–6, ESI: Fig. S7†). Also the crystallite sizes, specific surface areas and Zn contents of the resulting zincian malachite precursors were similar. Reducing the pH, however, strongly affected the mechanism of the aging process. Most striking is the absence of the sodium zinc carbonate phase at low pH associated with a delay of crystallization (Table 1, ID 1–3). Only for pH ≥ 7 sodium zinc carbonate was detected, while zincian malachite crystallized from the amorphous starting material at pH ≤ 6.5 without participation of any other EDXRD-detectable phase. The corresponding evolution of crystalline phases is presented in Fig. 6c for aging at pH 5 and as ESI for the other pH values (Fig. S7†). The decrease of intensity shown in Fig. 6c is probably due to partial dissolution of zincian malachite at a low pH value. Fig. 6g shows that $d_{20\bar{1}}$ is constant or even slightly increasing directly after the crystallization period suggesting that there is hardly any change of the Zn-content in zincian malachite with aging time for these samples. Thus, a second, simpler mechanism of aging is present with only one detectable step:

$$\mathrm{a-Cu_{0.7}(OH)_x(CO_3)_{0.7-x/2}\cdot Zn_{0.3}(OH)_y(CO_3)_{0.3-y/2}} \rightarrow \mathrm{(Cu_{>0.7}Zn_{<0.3})_2(OH)_2CO_3} + w\mathrm{Zn}\downarrow \quad (3)$$

It can be seen from Table 1 that this mechanism of crystallization seems kinetically hindered as longer isothermal induction periods are required compared to reactions following the mechanism of eqn (2) at the same temperature. The preferred Zn-sink phase Zn↓ for this mechanism can be identified as aurichalcite (Table 1).

Interestingly, despite the presence of significant amounts of aurichalcite, there was a significantly higher degree of Zn-incorporation into the resulting zincian malachite if crystallized in the absence of the sodium zinc carbonate according to eqn (3). Accordingly, *ex situ* XRD evaluation suggested the presence of two groups of precursors (Fig. 8): the precursors crystallized without sodium zinc carbonate obtained at low pH with large amounts of Zn incorporated into the cationic lattice of zincian malachite (small $d_{20\bar{1}}$, 28.4–29.2% Zn in zincian malachite) and the ones obtained at higher pH with significantly lower amounts of Zn on Cu-sites (large $d_{20\bar{1}}$, 26.0–26.3% Zn in zincian malachite). The overall Cu : Zn ratio of the recovered solid detected by XRF was always near the starting composition for all samples (Table 1) suggesting again that other non-detectable Zn-rich by-phases Zn↓ are present and act as a sink for Zn, in particular if crystallization occurred at high pH in the presence of sodium zinc carbonate. The highest Zn incorporation of this study was detected for the samples obtained at $T$ = 333 K and pH 5. According to Fig. 7, the Zn content of zincian malachite is 29.2%.

The successful minimization of any form of Zn segregation – like the transient crystallization of sodium zinc carbonate or the formation of the Zn-rich aurichalcite phase – helps to prepare a homogeneous precipitate capable of efficient nanostructuring during thermal decomposition according to the scheme presented in Fig. 1a.

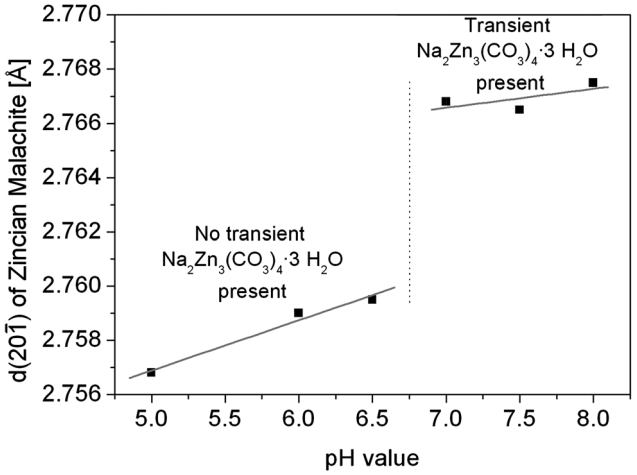


**Fig. 8** $d_{20\bar{1}}$ values of zincian malachite (from *ex situ* XRD) depending on the pH value of simulated aging. Two different groups can be observed: The zincian malachite samples crystallized without intermediate formation of sodium zinc carbonate (pH 5–6.5) show low $d_{20\bar{1}}$ values indicating a high Zn content. Crystallizations *via* the intermediate (pH 7–8) led to high $d_{20\bar{1}}$ values or low Zn content, respectively. Lines are guides for the eye.

### 3.5 The effect of potassium counter ions

In the case of the mechanism described by eqn (2), it is tempting to relate the lack of Zn in the zincian malachite precursor to the amount of Zn, which has intermediately formed the sodium zinc salt. In order to test this hypothesis, analogous experiments were performed using an aging solution based on neutralized $K_2CO_3$ solution. The absence of $Na^+_{aq}$ should suppress the formation of the transient sodium salt also at higher pH and therefore may have a promoting effect on the desired incorporation of Zn into zincian malachite under these conditions.

The experiments at pH 7 ($T$ = 333, 343 K) were repeated using $K_2CO_3$ instead of $Na_2CO_3$ in the aging medium (Table 1, ID 9, 10). As expected, no sodium zinc carbonate and no other by-phases were found in contrast to the aging experiment with $Na_2CO_3$ under the same conditions. This observation highlights the unexpected influence of the alkali metal counter ion on the chemistry of aging under these conditions. The crystallization of zincian malachite in the absence of $Na^+$ was strongly delayed (Fig. 6a and d *cf.* ID 4 and ID 9 F; Table 1, *cf.* ID 4, 8 and 9, 10). With the exception of the first two patterns, there was no significant down-shift in $d_{20\bar{1}}$ indicating the absence of any other transient Zn-storage phase (Fig. 6h). Surprisingly, although the transient formation of sodium zinc carbonate was suppressed, the final $d_{20\bar{1}}$ values of the resulting zincian malachite phase were comparable to those obtained with $Na_2CO_3$. The crystallization of (Cu-rich) malachite can happen faster if a transient storage phase for Zn can form, but the final degree of Zn incorporation into zincian malachite is similar at a given pH value. This indicates that Zn incorporation is rather determined by the acidity of the aging medium, *i.e.* by thermodynamics, than affected by the transient segregation chemistry, *i.e.* by kinetics. It is the availability of $H^+$, which seems to promote or limit the zinc incorporation into zincian malachite and balances the ratio of Zn deposited into the Zn-sink phase Zn↓ (Fig. 8) *via* the one or the

 This journal is © The Royal Society of Chemistry 2012

Downloaded by Fritz Haber Institut der Max Planck Gesellschaft on 19 February 2013
Published on 31 August 2012 on http://pubs.rsc.org | doi:10.1039/C2DT31236K

other pathway. The lower limit of the pH value is, however, given by the partial dissolution of $Zn^{2+}$ in an acidic environment leading to incomplete solidification[36] or leaching and unfavorable Zn distribution (*cf.* section 3.4).

## 4. Conclusion

The aging process of mixed Cu,Zn hydroxycarbonate precursors was decoupled from the precipitation and studied independently using *in situ* EDXRD and *in situ* UV-Vis spectroscopy. Crystalline zincian malachite, the desired precursor phase for Cu/ZnO catalysts, was successfully formed from the amorphous starting material in all experiments by aging in solutions with a composition near to the mother liquor under controlled co-precipitation conditions. As a function of different aging conditions, a variation of the Zn content in zincian malachite between *ca.* 24 and 29% was observed despite the same nominal Zn-content in the starting material of 30% indicating that a varying fraction of Zn was present in an undetected phase "Zn↓" acting as a sink for Zn. Two mechanisms to approach the maximal Zn incorporation into the zincian malachite catalyst precursor were observed: by direct co-condensation of $Cu^{2+}$ and $Zn^{2+}$ into Zn-rich malachite, or by first simultaneous crystallization of Cu-rich malachite and a transient Zn-storage phase, which in the course of aging re-dissolved and allows for later Zn-enrichment of malachite. The latter mechanism is favored at pH $\geq$ 7 in the presence of $Na^+$ leading to crystallization of sodium zinc carbonate as a Zn-storage phase. The former mechanism was observed at 5 $\geq$ pH $\geq$ 6.5 and yields a higher Zn-incorporation into zincian malachite. The radar plots shown in Fig. 9 summarize the effects of pH, temperature and alkali cations on the aging process. It can be seen that variation in pH changes the aging mechanism, while variation of temperature (at pH 7) leads to gradual changes. Thus, the acidity of the aging medium was identified as the most critical synthesis parameter to determine the final Zn-content in zincian malachite. Interestingly, Zn incorporation is independent of the crystallization mechanism. Even in the absence of $Na^+$, suppressing the transient crystallization of the sodium zinc carbonate storage phase, a lower degree of Zn incorporation was observed in the final sample at pH 7, although the reaction was following the direct co-condensation mechanism. The effect of individual synthesis parameters like temperature or acidity during catalyst preparation can be better rationalized on the basis of the complex chemistry of precursor aging. They should be optimized to give a low amount of Zn↓ and a maximal Zn-substitution in malachite approaching the nominal Cu : Zn ratio of the synthesis.

In general, this study shows that by dissecting coupled steps of precipitation reactions like solidification and aging, the influence of synthesis parameters on the target material can systematically be investigated for the individual steps. It furthermore highlights the value of careful *in situ* investigations to get insights into the crystallization and aging mechanisms of precipitated inorganic solids. Such insights are not only valuable for a retrospective understanding of empirically optimized synthesis recipes as reported here, but also have great potential for a further and more rational optimization of the preparation of this and other catalyst materials.

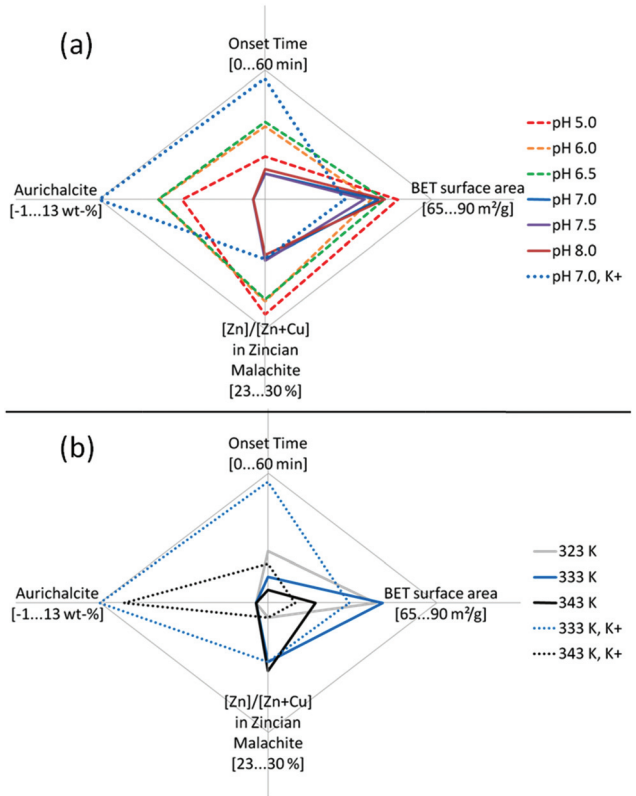


**Fig. 9** Radar plots illustrating the influence of the aging parameters pH value (a, at $T$ = 333 K) and temperature (b, at pH = 7) on the aging reaction and the properties of the resulting zincian malachite material. Variation of pH leads to different aging mechanisms below pH 6.5 (a, broken lines) and above pH 7 (a, full lines) and affects the Zn content of the catalyst precursor. Temperature leads to a gradual change of the aging kinetics (b, full lines). Substitution of $Na^+$ by $K^+$ in the aging solution at the same temperature (a, dotted lines) has a pronounced effect on the aging reaction and the phase composition, but not on the Zn content of the zincian malachite precursor. As a function of temperature, a variation of the Zn content is observed with $Na^+$ and $K^+$.

## Acknowledgements

This paper has emerged from a joint research project "Next generation methanol synthesis catalysts", which was funded by the German Federal Ministry of Education and Research (BMBF, FKZ 01RI0529). We acknowledge Edith Kitzelmann, Achim Klein-Hofmann, Gisela Lorenz, and Doreen Steffen for their substantial support in the lab, Elena Antonova, Jing Wang and Wolfgang Bensch for support with the EDXRD measurements, and HASYLAB (Hamburg, Germany) for allocation of beamtime. Martin Muhler and Stefan Kaluza are acknowledged for fruitful discussions. Robert Schlögl is greatly acknowledged for his continuous support.

## Notes and references

1 K. de Jong, *Synthesis of Solid Catalysts*, Wiley VCH, Weinheim, 2009.
2 M. Kurtz, N. Bauer, C. Buscher, H. Wilmer, O. Hinrichsen, R. Becker, S. Rabe, K. Merz, M. Driess, R. A. Fischer and M. Muhler, *Catal. Lett.*, 2004, **92**, 49–52.
3 C. Baltes, S. Vukojevic and F. Schüth, *J. Catal.*, 2008, **258**, 334–344.

View Article Online


4 B. Bems, M. Schur, A. Dassenoy, H. Junkes, D. Herein and R. Schlögl, *Chem.–Eur. J.*, 2003, **9**, 2039–2052.
5 I. Kasatkin, P. Kurr, B. Kniep, A. Trunschke and R. Schlögl, *Angew. Chem., Int. Ed.*, 2007, **46**, 7324–7327.
6 R. G. Herman, K. Klier, G. W. Simmons, B. P. Finn, J. B. Bulko and T. P. Kobylinski, *J. Catal.*, 1979, **56**, 407–429.
7 J. C. Frost, *Nature*, 1988, **334**, 577–580.
8 V. Ponec, *Surf. Sci.*, 1992, **272**, 111–117.
9 Y. Kanai, T. Watanabe, T. Fujitani, M. Saito, J. Nakamura and T. Uchijima, *Catal. Lett.*, 1994, **27**, 67–78.
10 N. Y. Topsoe and H. Topsoe, *Top. Catal.*, 1999, **8**, 267–270.
11 J. D. Grunwaldt, A. M. Molenbroek, N. Y. Topsoe, H. Topsoe and B. S. Clausen, *J. Catal.*, 2000, **194**, 452–460.
12 T. Ressler, B. L. Kniep, I. Kasatkin and R. Schlögl, *Angew. Chem., Int. Ed.*, 2005, **44**, 4704–4707.
13 M. Behrens, F. Studt, I. Kasatkin, S. Kühl, M. Hävecker, F. Abild-Pedersen, S. Zander, F. Girgsdies, P. Kurr, B.-L. Kniep, M. Tovar, R. W. Fischer, J. K. Nørskov and R. Schlögl, *Science*, 2012, **336**, 893–897.
14 D. Waller, D. Stirling, F. S. Stone and M. S. Spencer, *Faraday Discuss. Chem. Soc.*, 1989, **87**, 107–120.
15 S. Fujita, A. M. Satriyo, G. C. Shen and N. Takezawa, *Catal. Lett.*, 1995, **34**, 85–92.
16 D. M. Whittle, A. A. Mirzaei, J. S. J. Hargreaves, R. W. Joyner, C. J. Kiely, S. H. Taylor and G. J. Hutchings, *Phys. Chem. Chem. Phys.*, 2002, **4**, 5915–5920.
17 B. L. Kniep, T. Ressler, A. Rabis, F. Girgsdies, M. Baenitz, F. Steglich and R. Schlögl, *Angew. Chem., Int. Ed.*, 2004, **43**, 112–115.
18 M. Behrens, *J. Catal.*, 2009, **267**, 24–29.
19 A. M. Pollard, M. S. Spencer, R. G. Thomas, P. A. Williams, J. Holt and J. R. Jennings, *Appl. Catal., A*, 1992, **85**, 1–11.
20 M. Behrens and F. Girgsdies, *Z. Anorg. Allg. Chem.*, 2010, **636**, 919–927.
21 M. Behrens, F. Girgsdies, A. Trunschke and R. Schlögl, *Eur. J. Inorg. Chem.*, 2009, **10**, 1347–1357.
22 R. Kiebach, N. Pienack, M. E. Ordolff, F. Studt and W. Bensch, *Chem. Mater.*, 2006, **18**, 1196–1205.
23 L. Engelke, M. Schaefer, F. Porsch and W. Bensch, *Eur. J. Inorg. Chem.*, 2003, **3**, 506–513.
24 N. Pienack and W. Bensch, *Angew. Chem., Int. Ed.*, 2011, **50**, 2014–2034.
25 R. I. Walton and D. O'Hare, *Chem. Commun.*, 2000, 2283–2291.
26 A. Michailovski, J. D. Grunwaldt, A. Baiker, R. Kiebach, W. Bensch and G. R. Patzke, *Angew. Chem., Int. Ed.*, 2005, **44**, 5643–5647.
27 M. Behrens, R. Kiebach, J. Ophey, O. Riemenschneider and W. Bensch, *Chem.–Eur. J.*, 2006, **12**, 6348–6355.
28 F. Porsch, *EDXPowd, 3.155*, RTI GmbH, Paderborn, Germany, 2004.
29 L. Engelke, M. Schaefer, M. Schur and W. Bensch, *Chem. Mater.*, 2001, **13**, 1383–1390.
30 A. Coelho, *TOPAS, 4.2*, Bruker AXS GmbH, Karlsruhe, Germany, 2003–2009.
31 T. E. Gier, X. H. Bu, S. L. Wang and G. D. Stucky, *J. Am. Chem. Soc.*, 1996, **118**, 3039–3040.
32 F. Zigan, W. Joswig, H. D. Schuster and S. A. Mason, *Z. Kristallogr.*, 1977, **145**, 412–426.
33 S. Kaluza, M. Schröter, R. d'Alnoncourt, T. Reinecke and M. Muhler, *Adv. Funct. Mater.*, 2008, **18**, 3670–3677.
34 H. Jung, D.-R. Yang, O.-S. Joo and K.-D. Jung, *Bull. Korean Chem. Soc.*, 2010, **31**, 1241–1246.
35 S. Klokishner, M. Behrens, O. Reu, G. Tzolova-Müller, F. Girgsdies, A. Trunschke and R. Schlögl, *J. Phys. Chem. A*, 2011, **115**, 9954–9968.
36 J. L. Li and T. Inui, *Appl. Catal., A*, 1996, **137**, 105–117.
37 M. Behrens, D. Brennecke, F. Girgsdies, S. Kissner, A. Trunschke, N. Nasrudin, S. Zakaria, N. F. Idris, S. B. Abd Hamid, B. Kniep, R. Fischer, W. Busser, M. Muhler and R. Schlögl, *Appl. Catal., A*, 2011, **392**, 93–102.


Downloaded by Fritz Haber Institut der Max Planck Gesellschaft on 19 February 2013
Published on 31 August 2012 on http://pubs.rsc.org | doi:10.1039/C2DT31236K


This journal is © The Royal Society of Chemistry 2012